ACS APPLIED MATERIALS & INTERFACES

Research Article

www.acsami.org

$NaGdF_4:Yb^{3+}/Er^{3+}@NaGdF_4:Nd^{3+}@Sodium\text{-}Gluconate$: Multifunctional and Biocompatible Ultrasmall Core–Shell Nanohybrids for UCL/MR/CT Multimodal Imaging

Dandan Ma,[†] Lingjie Meng,[†] Yuzhong Chen,[†] Min Hu,[*,†] Yanke Chen,[‡] Chen Huang,[*,‡] Jin Shang,[§] Ruifeng Wang,[§] Youmin Guo,[§] and Jian Yang[§]

[†]Department of Applied Chemistry, School of Science, Xi'an Jiaotong University, Xi'an 710049, China

[‡]Key Laboratory of Environment and Genes Related to Diseases, College of Medicine, Xi'an Jiaotong University, Xi'an 710061, China

[§]Department of Diagnostic Radiology, The First Affiliated Hospital of Xi'an Jiaotong University, Xi'an 710061, China

Supporting Information

ABSTRACT: Multimodal bioimaging nanoparticles by integrating diverse imaging ingredients into one system, represent a class of emerging advanced materials that provide more comprehensive and accurate clinical diagnostics than conventional contrast agents. Here monodisperse and biocompatible core–shell nanoparticles, $NaGdF_4$: Yb^{3+}/Er^{3+}@$NaGdF_4$:Nd@sodium-gluconate (termed as GNa-Er@Nd), with about 26 nm in diameter were successfully prepared by a facile two step reactions in high boiling solvents, and followed a ligand exchange process with sodium gluconate. The resulting GNa-Er@Nd nanoparticles were well characterized by transmission electron microscopy (TEM), X-ray diffraction (XRD), Fourier transform infrared spectra (FTIR), and zeta potentials. These nanohybrids present brightly dual-wavelength excited upconversion luminescence (UCL) under both 980 and 793 nm laser because of the synergistic effect of Yb^{3+}/Er^{3+} and Nd^{3+}. They also exhibited excellent relaxivity parameters (r_1) in magnetic resonance imaging (MRI) and Hounsfield units (HU) in X-ray computed tomography (CT) that are comparable to the clinical contrast agents. Therefore, these small and monodisperse nanoparticles provide options to construct a unique platform for potential multimodal UCL/CT/MRI imaging simultaneously.

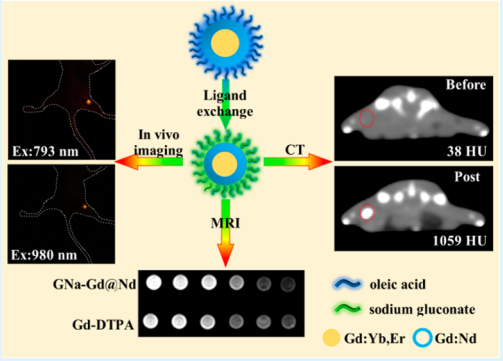

KEYWORDS: *upconversion nanoparticles, sodium-gluconate, core–shell, biocompatibility, multimodal imaging*

1. INTRODUCTION

Multimodal imaging materials have recently attracted significant attention for clinical molecular imaging and diagnostics because they could inherit diverse imaging features from multimodal functionality and complementary each other to significantly improve the sensitivity of existing diagnostic technique.[1−4] The frequently used imaging technologies for clinical diagnosis include fluorescence imaging, X-ray computed tomography (CT), magnetic resonance imaging (MRI), positron emission tomography (PET), and ultrasonic imaging.[5−8] Fluorescence imaging provides the highest spatial resolution (even tens of nanometers), and can be used to monitor a broad range of biological activities and even to study the structure–activity relationship of biomolecules. But it is difficult for fluorescence imaging to obtain accurate anatomical and physiological information in the in vivo experiments due to the limited depth of penetration in tissues.[9,10] Whereas, ultrasound, CT, MRI and PET can provide exceptional 3D anatomical information with different spatial resolution base on the situations of the different organs and tissues.[1,5] Multimodal imaging, combining two or more imaging modality such as CT, MRI, PET and fluorescence imaging in one system, takes great promising to bridge gaps in resolution and penetration depth. For example, Cameron et al. combined fluorescence probe (rhodamine B) with magnetic Fe_3O_4 nanospheres to simultaneously realize fluorescence imaging and MRI.[11] Lydia groups developed another nanohybrid systems composed of superparamagnetic Fe_3O_4 and ^{99m}Tc for concurrent MR and CT contrast imaging.[12] In theory, thousands of combinations of various imaging components, drugs and even targeting molecules could be designed and prepared to meet multifunction and high performance. However, multifunctional particles often mean that they have complex structures, large size, time-consuming multistep preparation and bad repetitiveness. Only the small nanoparticles (generally <120 nm) with proper surface modification prefer to be delivered to and act at the disease sites. Therefore, it is an ongoing challenge to develop facile methods to construct multimodal imaging materials that are small, monodisperse as well as water dispersible and biocompatible.

Received: March 24, 2015
Accepted: July 10, 2015
Published: July 10, 2015

DOI: 10.1021/acsami.5b05194
ACS Appl. Mater. Interfaces 2015, 7, 16257−16265

The lanthanide-doped upconversion nanoparticles (UCNPs) can transfer low-energy near-infrared (such as 980 nm) photons into high-energy visible photons via multiphoton processes.[13−17] They are regarded as a class of ideal fluorescent materials for bioimaging and biodetection, because they have appropriate emission/excitation wavelengths to minimize the strong scattering, absorption and damage in tissues and thus provide deep penetration in tissue, high signal-to-noise ratio.[18−20] In addition, they also showed good photostability, and a large spectral shift due to their ability to efficiently upconvert NIR radiation into shorter wavelengths. The "optical transparency window" of biological tissues ranges from 650 to 1100 nm often allows a deeper light penetration and lower autofluorescence.[21−24] Therefore, Nd^{3+} ions are quite attractive because of their absorption bands at around 800 nm and emission peaks at 900−1100 nm. Recently, it was found that the Yb^{3+}/Nd^{3+} cosensitized nanoparticles can be excited by dual-wavelength laser of both 980 and 808 nm.[25,26] The dual-wavelength excited imaging could achieve more accurate positioning and more sensitive diagnose compared to the single wavelength excited imaging.[27,28] For the lanthanide elements, it is also very interesting of Gd for the T_1 MRI because of the seven unpaired electrons in a Gd^{3+}.[29] Zhou's group first reported the $Tm^{3+}/Er^{3+}/Yb^{3+}$ codoped $NaGdF_4$ nanophosphors for luminescence and magnetic imaging.[30] Deng groups synthesized the Ho^{3+}-doped $NaGdF_4$ nanoparticles for MRI and optical brain glioma imaging.[31]Chen et al. synthesized $NaYbF_4$: $Tm^{3+}/NaGdF_4$ core−shell nanoparticles with photoluminescence and magnetic properties.[32] In addition, all lanthanide elements (from lanthanum to lutetium) possess potential X-ray attenuation properties for the nature of heavy atoms.[33,34] All of these excellent properties make the lanthanide-doped UCNPs attractive and be widely studied in multimodal imaging,[35−39] Therefore, we proposed a kind of core−shell $NaGdF_4:Yb^{3+}/Er^{3+}@NaGdF_4:Nd^{3+}$ (denoted as Er@Nd) nanoparticles that should be excited by both of 980 and 808 nm and emit upconversion fluorescence. Combined magnetic properties of Gd^{3+} and the X-ray attenuation properties of lanthanide atoms, these core−shell particles might have remarkable potential for multimodal fluorescence/CT/MRI imaging.

Herein, the monodisperse and well-defined core−shell Er@Nd nanoparticles with 26 nm in size were prepared by a facile two step reactions at 300 °C in the mixture of oleic acid and 1-octadecene. To improve the water-solubility and biocompatibility of Er@Nd nanoparticles, Sodium gluconate (GNa), a nonpoisonous multihydroxyl organic molecule with excellent water-solubility and biocompatibility, were modified on the surface of Er@Nd by a ligand exchange method. The successfully preparation of the resulting $NaGdF_4$:Yb/Er@$NaGdF_4$:Nd@GNa nanoparticles (denoted as GNa-Er@Nd) were systematically characterized by transmission electron microscopy (TEM), X-ray diffraction (XRD), Fourier transform infrared spectra (FTIR) and Zeta potentials. As respected, GNa-Er@Nd nanohybrids not only present brightly dual-wavelength excited upconversion luminescence (UCL) under both 980 and 793 nm laser, but also exhibited excellent relaxivity parameters (r_1) in MRI and Hounsfield units (HU) in CT. These small and disperse nanoparticles give great potentials for integrating dual-wavelength excited UCL/CT/MRI capacity into one nanoparticle system.

2. EXPERIMENTAL SECTION

2.1. Materials. $GdCl_3·6H_2O$ (99.99%), $YbCl_3·6H_2O$ (99.99%), $ErCl_3·6H_2O$ (99.99%), $NdCl_3·6H_2O$ (99.99%), and NaF (98.0%), were purchased from Sigma-Aldrich Co. 1-octadecene (90%), sodium gluconate (99%), and oleic acid (98%) were obtained from TCI. Arsenazo III was purchased from Shaanxi keyi Science & Technology Co., Ltd. HNO_3 (65 wt %, Guaranteed reagent) was purchased from Sinopharm Chemical Reagent Co., Ltd. The hepatoma carcinoma cell line SMMC-7721 was purchased from the Cell Resource Centre of Life Sciences. Fetal bovine serum (FBS), and Dulbecco's modified Eagle medium (DMEM) were obtained from Gibco BRL. Cell Counting Kit (CCK-8) was purchased from Shanghai Seven Sea Biological Technology Co., Ltd., Omniscan (Gd-DTPA), and iopromide were purchased from GE pharm., Co., in Shanghai. All other chemicals and solvents were obtained from Adamas-beta, Inc. (Shanghai, China). All chemicals and materials were used as received without further purification. Deionized water with resistivity of 18.2 MΩ was used throughout.

2.2. Synthesis of $NaGdF_4:Yb^{3+}/Er^{3+}$ Nanoparticles. In a typical experiment, $NaGdF_4:Yb^{3+},Er^{3+}$ nanoparticles were synthesized according to a reported method with some modifications.[42] In brief, $GdCl_3·6H_2O$ (0.815 mmol), $YbCl_3·6H_2O$ (0.18 mmol), and $ErCl_3·6H_2O$ (0.005 mmol) were added into the mixture of OA (5.5 mL) and 1-octadecene (4.5 mL) and stirred at 130 °C for 1 h until a clear solution was formed. After addition of NaF (40 mmol), the mixture was reacted at 300 °C for another 1 h with stirring. The resulting nanoparticles were precipitated by addition of ethanol (10 mL), collected by centrifugation and washed with ethanol (3× 10 mL) and *n*-hexane (3 × 10 mL), respectively. $NaGdF_4:Yb^{3+}/Er^{3+}$ nanoparticles were finally dispersed in *n*-hexane (5 mL).

2.3. Synthesis of Er@Nd Nanoparticles. The core−shell Er@Nd nanoparticles were synthesized by using a similar procedure to that of $NaGdF_4:Yb^{3+}/Er^{3+}$ cores. Typically, $GdCl_3·6H_2O$ (0.8 mmol) and $NdCl_3·6H_2O$ (0.2 mmol) were dissolved in the mixture of OA (5.5 mL) and 1-octadecene (4.5 mL) at 130 °C by stirring for 1 h. After it was cooled down to 50 °C, $NaGdF_4:Yb^{3+}/Er^{3+}$ nanoparticles solution in *n*-hexane (1 mmol) was added along with NaF (4 mmol) and then heated at 100 °C to remove *n*-hexane. The mixture was subsequently heated at 300 °C for another 1 h. The Er@Nd nanoparticles were isolated by centrifugation and washed with ethanol (3 × 10 mL) and *n*-hexane (3 × 10 mL). The obtained Er@Nd nanoparticles were dispersed in *n*-hexane (5 mL) for further use.

2.4. Surface modification of Er@Nd with GNa. The hydrophobic Er@Nd nanoparticles capped by oleic acid were transferred to the aqueous phase via a simple ligand-exchange method. Er@Nd hexane solution (10 mg/mL, 1 mL) was added to diluted hydrochloric acid (pH = 4, 10 mL) and shaken gently for 1 h to obtain ligand-free Er@Nd nanoparticles. The ligand-free Er@Nd nanoparticles were collected by centrifugation and redispersed in sodium gluconate (GNa) solution (5 mg/mL, 5 mL) and heated at 50 °C for another 5 h. Finally, the resulting GNa-Er@Nd nanoparticles were washed with deionized water (3 × 5 mL) by repeated sonication and centrifugation.

2.5. Leaching Studies of Gd^{3+} from the GNa-Er@Nd Nanoparticles. Arsenazo III was used to check the leaking of the Gd^{3+}.[40,41] The GNa-Er@Nd nanoparticles were dispersed in PBS solution (6 mg/mL) and kept at 37 °C for 7 days. The GNa-Er@Nd nanoparticles were removed by centrifugation for 30 min at 10000 r/min. The supernatant was then incubated with 0.05 mM Arsenazo III and analyzed the presence of Gd^{3+} by monitoring the absorption at 658 nm.

2.6. Cytotoxicity Assay. The cytotoxicity of GNa-Er@Nd nanoparticles were studied on SMMC 7721 cells by CCK-8 assay. The SMMC 7221 cells were plated in 96-well flat-bottomed plates with a concentration of 5×10^4 cells per well and allowed to culture in RPMI 1640 (Roswell Park Memorial Institute's Medium) supplemented with 10% FBS at 37 °C in a humidified incubator in which the CO_2 level was maintained constant at 5%. After culturing overnight, the cells were washed with FBS-free RPMI 1640 solutions and incubated with a specific concentration of GNa-Er@Nd (50, 100, 200,

DOI: 10.1021/acsami.5b05194
ACS Appl. Mater. Interfaces 2015, 7, 16257−16265

400 mg/mL) in FBS-free RPMI 1640 solution (100 μL/well) for 12, 24, and 48 h at 37 °C. Subsequently, CCK-8 reagent (5 mg/mL, 10 μL) was added to each well and incubated for additional 4 h at 37 °C. The absorbance was then measured at 450 nm using a monochromator-based multifunction microplate reader.

2.7. In Vivo Upconversion Imaging. Female nude BALB/c mice (aged 7−8 weeks, weighing 20.0 ± 2.0 g) were kept in the facility with free access to food and water. SMMC 7221 cells (1×10^7 cells per mouse) were inoculated into the right hind limbs of nude mice. When the tumors grew to the size of 100−300 mm^3, GNa-Er@Nd nanoparticles (50 uL, 10 mg/mL in normal saline) were in situ injected into the tumor position of a nude mouse which had been anesthetized with 10% chloral hydrate. Upconversion bioimagings were detected after 15 min injection under the excitation of 980 and 793 nm laser separately by using a digital camera (Canon). A short pass filter (705 nm) was used to eliminate the interference of the excitation light of 793 nm.

2.8. In Vitro and in Vivo X-ray CT Imaging. The in vitro CT imaging was first carried on a Philips 256-slice CT scanner at 120 kVp voltages. A series of aqueous solutions of GNa-Er@Nd (0 to 20 mg/mL) in 2.0 mL Eppendorf tubes were prepared. The 3D data sets were reconstructed with a voxel size of 20 μm. To perform in vivo CT imaging, a tumor-bearing nude mouse was first anesthetized with 10% chloral hydrate. GNa-Er@Nd (100 μL, 10 mg/mL) were intratumorally injected into the tumor in situ. The mouse was scanned on a Philips 256-slice CT scanner before and after the injection. CT imaging parameters were given as follows: Slice thickness of 0.9 mm, pitch of 0.99, 120 kVp, 300 mA, field of view with 350 mm, gantry rotation time of 0.5 s; table speed of 158.9 mm s^{-1}. The insection axial images were reformed to coronal images by a computational technique referred to as multiplanar reconstruction.

2.9. T_1-Weighted MR Imaging. A series of aqueous solutions of GNa-Er@Nd particles (0−0.5 mmol Gd) in 2.0 mL Eppendorf tubes were investigated in a 3.0 T MR scanner. The parameters for T_1 measurements were set as follows: echo time (TE) = 15.3 ms; repetition time (TR) = 500, 1000, 1500, 2000 ms; number of excitations (NEX) = 8. T_1 measurements were performed using a nonlinear fit to changes in the mean signal intensity within each well as a function of repetition time. Finally, the relaxivity values (R_1) were determined through the curve fitting of $1/T_1$ relaxation time (s^{-1}) versus the Gd concentration (mM).

2.10. Characterizations. Transmission electron microscopy (TEM) analysis was carried out on a JEOL-1400 transmission electron microscope operating at 100 kV and high-resolution TEM (HRTEM) images were obtained using a JEOL-JEM 2010 F field emission transmission electron microscope operated at an acceleration voltage of 200 kV. The size and distribution of all as-prepared nanomaterials were determined from TEM micrographs using ImageJ (V1.41, NIH, USA) for image analysis. XRD patterns were collected on a powder diffractometer (D/max-2200/PC, Rigaku, Japan) using Cu−K irradiation (40 kV, 20 mA). Diffraction patterns were collected from15° to 70° at a speed of 3°·min^{-1}. Fourier transform infrared (FTIR) spectra were acquired in the spectral range from 4000 to 400 cm^{-1} with Bruker Sensor S7 by using pressed KBr tablets. Zeta-potential experiments and hydrodynamic diameter were determined on Malvern Zetasizer 3000 HS at 25 °C. The contents of rare earth elements in the GNa-Er@Nd nanoparticles were measured using ICP-MS analysis (Thermo XSERIES II). The absorption curves were obtained by UV-2550 UV−vis spectrophotometer (Shimadzu). Photoluminescence (PL) spectra were recorded at room temperature with an F-4600 spectrophotometer (Hitachi) with the excitation source adapted to fiber coupled diode lasers. Unless otherwise stated, all spectra were obtained from *n*-hexane. Dispersion of nanoparticles (0.5 wt %) at an excitation laser power of 500 mW. Luminescence digital photographs were taken with a Nikon D90 camera. CT imaging was obtained at 120 kVp voltages on a Philips 260-slice CT scanner (Philips Medical System). T_1 relaxation time was conducted by PQ001 MRI Analyst (Shanghai Niumag Corporation, China). T_1-weighted images were measured by NMI20-Analyst (Shanghai Niumag Corporation, China). MR imaging experiments were performed in a 3.0 T MR scanner (GE signa HDxt, Milwaukee, WI).

3. RESULTS AND DISCUSSION

3.1. Synthesize of GNa-Er@Nd Nanoparticles. The synthesis of GNa-Er@Nd core−shell nanoparticles is a relatively straightforward process (Figure 1). $NaGdF_4$:Yb^{3+}/Er^{3+} nanoparticles were first synthesized by heating the $GdCl_3 \cdot 6H_2O$, $YbCl_3.6H_2O$ and $ErCl_3.6H_2O$ in the mixture of OA and 1-octadecene at 300 °C with the presence of NaF. The relatively high reaction temperature benefits the high crystalline of nanoparticles in the high boiling solvent mixture of OA and 1-octadecene. The Er@Nd core-shell nanoparticles were further synthesized via a seed mediated growth process. The $NaGdF_4$:Nd^{3+} shells can not only isolate the active ions (Yb^{3+}/Er^{3+}) in the cores from the environment to improve the luminescence, but also provide another luminescence channel under irradiation of 793 nm by transferring 793 nm energy to Yb^{3+}. During the two-step reaction process, oleic acid (OA) acted as both solvent and surface capping agents. The resulting Er@Nd nanoparticles can only disperse well in nonpolar organic solvents such as in *n*-hexane because of the hydrophobic nature of OA. However, good water-solubility and biocompatibility are always necessary for any biomaterials before they used in biotechnology and medicine fields. Therefore, a facile ligand exchange method was employed to transfer Er@Nd nanoparticles into water by replacing OA with water-soluble ligands such as GNa. In addition, the hydroxyl and carboxyl groups on GNa endowed the GNa-Er@Nd nanoparticles tailored surface chemistry for covalent coupling targeted substances and drugs, which could further expand their applications in medicine and biological field.

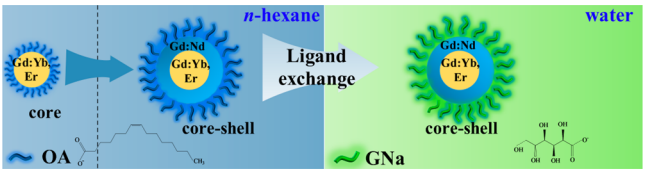

Figure 1. Scheme for the preparation of hydrophilic GNa-Er@Nd nanoparticles.

3.2. Characterizations of GNa-Er@Nd Nanoparticles. Transmission electron microscopy (TEM) was employed to investigate the morphology and structures of the as-synthesized nanoparticles (Figure 2). The $NaGdF_4$:Er^{3+}/Yb^{3+} nanoparticles are well monodisperse with a diameter of 19 ± 2 nm (Figure 2a and b). After the $NaGdF_4$:Er^{3+}/Yb^{3+} cores were coated by $NaGdF_4$:Nd^{3+} shell, the size of Er@Nd nanoparticles increased to 26 ± 2 nm with a narrow size distribution (Figure 2c and d). Therefore, the average thickness of the $NaGdF_4$:Nd^{3+} shell was about 3.5 nm. However, the core-shell structure cannot be clearly observed due to the similar electron contrast of shell and cores. GNa-Er@Nd nanoparticles exhibit uniform morphology and good monodispersity in water with a similar size to that of Er@Nd nanoparticles (Figure 2e and f). It indicates that the ligand exchange process did not change the morphology and size of Er@Nd nanoparticles. It is vital to control the size of nanomedicines (<120 nm) for cellular delivery, especially for in vivo experiments. The ultrasmall GNa-Er@Nd nanoparticles (26 nm) are small enough for bioimaging.

DOI: 10.1021/acsami.5b05194
ACS Appl. Mater. Interfaces 2015, 7, 16257−16265

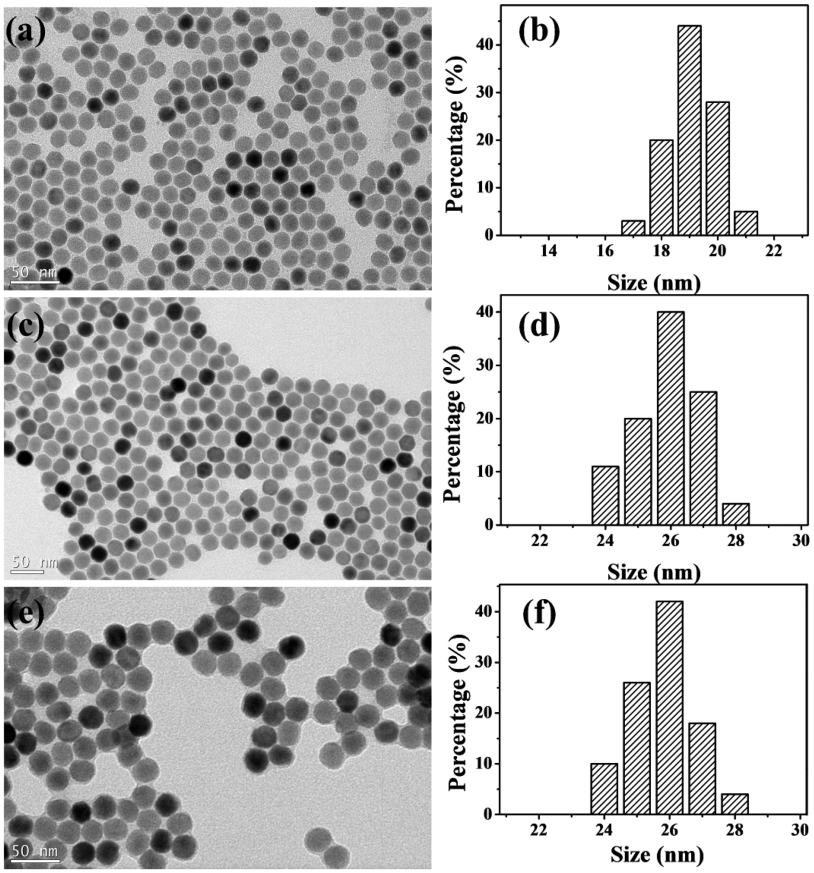

Figure 2. TEM images and the size distribution of (a,b) $NaGdF_4$:Yb^{3+}/Er^{3+}, (c,d) Er@Nd nanoparticles, and (e,f) GNa-Er@Nd.

The crystal structures of the as-obtained $NaGdF_4$:Yb^{3+}/Er^{3+} and Er@Nd nanoparticles were studied by XRD (Figure 3). All

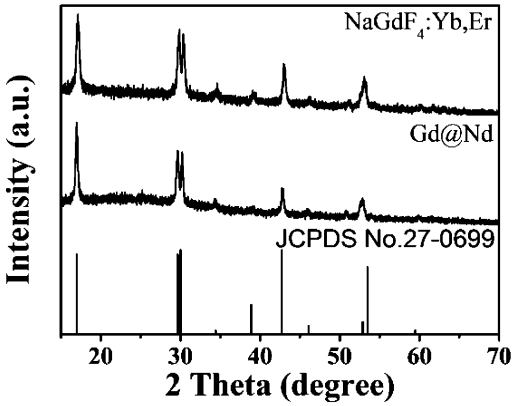

Figure 3. X-ray diffraction patterns of $NaGdF_4$:Yb^{3+}/Er^{3+} and Er@Nd nanoparticles.

the identified diffraction peaks for these two samples in the XRD pattern were in good agreement with the hexagonal phase of $NaGdF_4$ (JCPDS card no. 27−0699). The doped Nd^{3+}, Yb^{3+} and Er^{3+} did not change the crystalline phase as their ionic radius is similar to Gd^{3+}. No impurity crystalline phase was found in the diffraction pattern, indicating the high phase purity of as-prepared nanocrystals. It should be noted that the $NaGdF_4$:Yb^{3+}/Er^{3+} nanoparticles with hexagonal phase structures generally exhibit much higher upconversion efficiency than their cubic phase counterpart.[1−4] Therefore, the narrowing diffraction peaks of Er@Nd nanoparticles suggest a good crystallinity that should be good for upconversion luminescence. The actual contents of rear-earth ions in the as synthesized GNa-Er@Nd nanoparticles were further measured using ICP-MS (Table S1). All the measured values agreed well with the theoretical values, indicating that the target products with precise contents were obtained.

Er@Nd nanoparticles could be well dispersed in *n*-hexane because the nanoparticle surfaces were capped by hydrophobic OA, whereas the GNa-Er@Nd nanoparticles showed excellent water solubility (Supporting Information Figure S1) because of the hydrophilic nature of GNa. It suggests that the hydrophobic nanoparticles have been converted into hydrophilic nanoparticles. The successful surface modification was further characterized by FTIR spectroscopy (Figure 4a). For the Er@Nd nanoparticles, the peaks at 2926 and 2855 cm^{-1} correspond to the symmetric and asymmetric stretching vibration of $-CH_2$ in OA ligand, while the band at 1553 cm^{-1} arises from the stretching asymmetric vibration of free −COOH in OA (red line in Figure 4a). As for the GNa-Er@Nd (black line in Figure 4a), it is obvious to see a broad band at around 3479 cm^{-1} and a weak peak at 1618 cm^{-1}, which can be ascribed to the vibration of O−H and the C═O, the sharp bands at 1076 cm^{-1} is the vibration of C−O. These three peaks are the characteristic peaks of GNa, which suggested that the Er@Nd have been successfully modified with the ligands of GNa. The hydrodynamic diameters of GNa-Er@Nd nanoparticles were monitored to check the suspension stability (Figure 4b). The hydrodynamic diameters of GNa-Er@Nd nanoparticles were kept at about 150 nm and showed negligible

DOI: 10.1021/acsami.5b05194
ACS Appl. Mater. Interfaces 2015, 7, 16257−16265

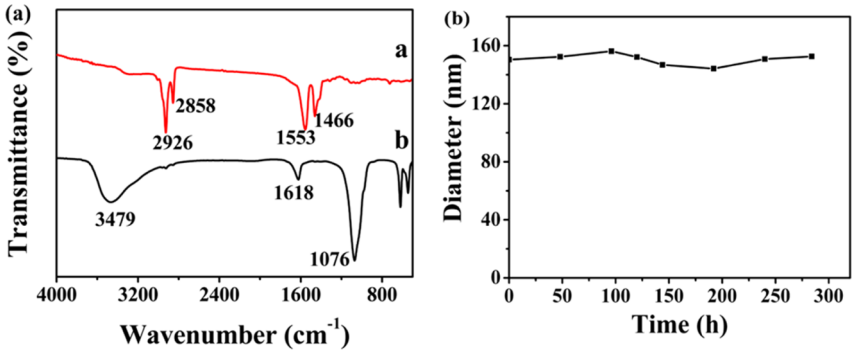

Figure 4. (a) The FTIR spectra of Er@Nd (red line) and GNa-Er@Nd (black line). (b) Temporal evolutions of the hydrodynamic diameter of GNa-Er@Nd nanoparticles in water.

change in more than 10 days. The zeta potential of ligand-free Er@Nd nanoparticles is about 40 mV. And, the zeta potential of GNa-Er@Nd nanoparticles declined to 20 mV and fluctuates in a narrow range about 400 h (Supporting Information Figure S2). Therefore, the GNa ligands can well adsorb onto the surfaces of Er@Nd nanoparticles and effectively prevent their aggregation in water.

3.3. Cytotoxicity of GNa-Er@Nd Nanoparticles. Any biomaterials are expected to have an intrinsically low toxicity; the SMMC-7721 cells were assayed for the quantitative assessment of the cytotoxicity of GNa-Er@Nd nanoparticles by using standard CKK-8 assay (Figure 5). The SMMC-7721

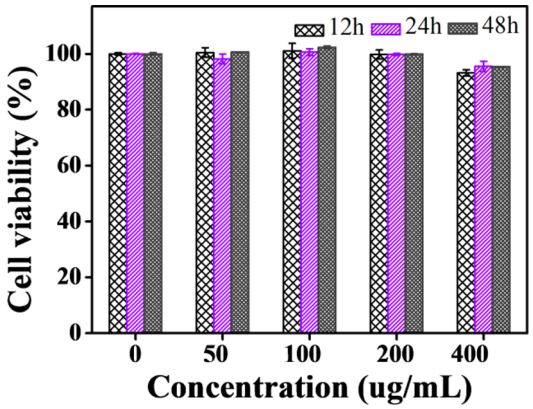

Figure 5. Viability of SMMC-7721 cells incubated with GNa-Er@Nd (50−400 μg/mL) for 12, 24, and 48 h by the standard CCK-8 assay.

cells incubated with GNa-Er@Nd nanoparticles did not result in any obvious cytotoxicity over a wide concentration range (0−400 μg/mL) for 12, 24, and 48 h. Cell viability was higher than 90% for all cases, indicating negligible biological toxicity of GNa-Er@Nd nanoparticles. Because the Gd^{3+} have obvious toxicity, we further confirmed that there is ignorable Gd^{3+} leakage in the physiological conditions after the GNa-Er@Nd nanoparticles (6 mg/mL) dispersed in PBS solution for 7 days (Supporting Information Figure S3). As a result, GNa-Er@Nd nanoparticles should be safely used for bioimaging due to the presence of biocompatible GNa ligands.

3.4. Luminescence and Bioimaging in Vivo of GNa-Er@Nd Nanoparticles. Because the luminescence of rare earth ions is closely related with their environment, the luminescence properties of $NaGdF_4$:Yb^{3+}/Er^{3+}, Er@Nd and GNa-Er@Nd nanoparticles under the excitation of 980 and 793 nm laser were compared (Figure 6). Under the excitation of 980 nm, all the three nanoparticles have three UCL bands at 525, 540 and 656 nm (Figure 6a), corresponding to the transition of Er: $^2H_{11/2} \rightarrow {}^4I_{15/2}$, $^4S_{3/2} \rightarrow {}^4I_{15/2}$, and $^4F_{9/2} \rightarrow {}^4I_{15/2}$, respectively. Compared with the $NaGdF_4$:Yb^{3+}, Er^{3+} nanoparticles, core−shell nanoparticles with 20% Nd^{3+} doped in the shell layer can provide dramatic enhancement of luminescence intensity. This is mainly because the shell layer can efficiently avoid surface quenching of pure core and separate the surface luminescence center from solvent molecules. Interestingly, GNa-Er@Nd nanoparticles showed no significant luminescence quenching even being dispersed in water (Supporting Information Figure S1), suggesting a great potential for bioimaging.

The $NaGdF_4$:Yb^{3+}/Er^{3+} nanoparticles almost have not shown UCL under the excitation of 793 nm laser (Figure 6b). Whereas, Er@Nd and GNa-Er@Nd nanoparticles showed strong UCL at 525, 540, and 656 nm, which corresponding to

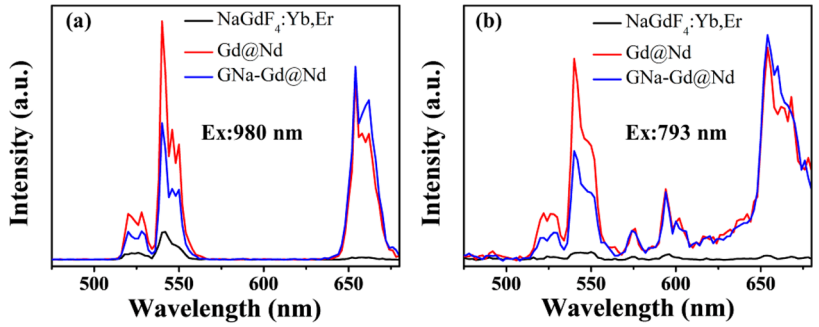

Figure 6. Upconversion emission spectra of the synthesized $NaGdF_4$:Yb^{3+}/Er^{3+}, Er@Nd and GNa-Gd@Nd nanoparticles under the excitation of 980 (a) and 793 nm (b). (Laser power is 500 mW; the concentration of samples is 0.5 mg/mL.)

DOI: 10.1021/acsami.5b05194
ACS Appl. Mater. Interfaces 2015, 7, 16257−16265

the emission bands under the excitation of 980 nm laser. In addition, an extra emission band was observed at about 600 nm, corresponding to $^4G_{7/2} \rightarrow {}^4I_{11/2}$ energy transition of Nd^{3+}. It indicates that the doped Nd^{3+} in the shell layer can harvest energy of 793 nm laser and get upconversion luminescence through Nd^{3+}-Yb^{3+}-Er^{3+} energy transfer process.[43] Obviously, the strong dual-wavelength excited UCL properties of Er@Nd nanoparticles provide alternative excitation light source in upconversion luminescence and promise to meet the needs of biological optical applications, such as accurate positioning, multiple tissue imaging and so on.[44]

On the basis of its dual-modal luminescence performance and low cytotoxicity, the applications of GNa-Er@Nd nanoparticles for fluorescence imaging in vivo were studied. The tumor bare nude BALB/c mice were injected with GNa-Er@Nd nanoparticles subcutaneously (10 mg/mL, 50 μL). The images were collected with an optical camera under natural light (Figure 7a) or excitation under 980 (Figure 7b) and 793 nm laser (Figure 7c) respectively. Because of the "optical transparency window" of biological tissues range from 650 to 1100 nm, the yellow-red light has deeper light penetration in tissues. Therefore, obvious yellow-red light could be seen at the injection positions of nude mouse with the naked eye under irradiation of 980 and 793 nm lasers. The dual-wavelength excited UCL imaging in vivo demonstrates the proof-of-concept of the GNa-Er@Nd, which can broaden choice of the illuminant in UCL imaging.

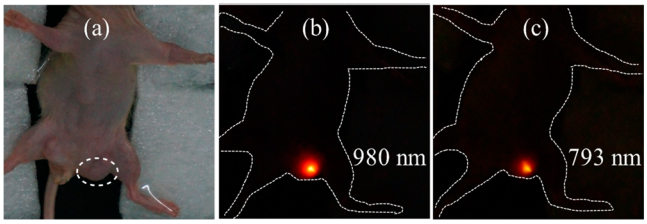

Figure 7. Whole-body image of a nude mouse injected via tumor mass in site with the GNa-Er@Nd nanocrystals under the excitation of natural light (a), 980 nm laser (b), and 793 nm laser (c). Injection site was marked with a black circle.

3.5. CT Imaging Experiments. Compared with UCL imaging, CT imaging can provide more spatial resolution information.[6] Because of the special heavy atoms effect of lanthanide elements, the GNa-Er@Nd nanoparticles possess potential X-ray attenuation properties in CT imaging. The ex vivo CT imaging of GNa-Er@Nd nanoparticles was first investigated. Different concentrations of GNa-Er@Nd nanoparticles were monitored by X-ray CT to determine the Hounsfield units (HU) value, using the control commercial X-ray imaging agent (Iopromide injection solution) as controls. As shown in Figure 8a, there are good linear relationships between concentrations of all samples and their values of HU, the slope of each line reflects the contrast effect of each sample. The slope of GNa-Er@Nd is 8.258, which is a bit higher than clinic contrast agent Iopromide (7.446), suggesting that the GNa-Er@Nd nanoparticles have superiority than Iopromide as CT imaging agents.

The CT experiments in vivo were further performed by intratumorally injecting the solution of GNa-Er@Nd (10 mg/mL, 50 μL) into the tumor site of a tumor bearing nude mouse (Figure 8b). The CT value of the tumor site is 38 HU, but the value significantly increased to 1059 HU after injection. The obvious enhancement of signal further indicates that the GNa-Er@Nd is efficiently in vivo CT imaging in particle.

3.6. MRI Imaging Experiments. Magnetic nanoparticles have been attracting much attention because of their potential as contrast agents for MR imaging. There are two kinds of contrast agents used in MRI. One is T_1 contrast agents (e.g., Gd-DTPA), which positively increase effect on T_1-weighted sequences and lead to bright signal enhancement. The other is T_2 contrast agents (e.g., Fe_3O_4) which negatively increase effect on T_2-weighted sequences and results in dark signal enhancement. However, the dark signals coming from not only the T_2 contract agents but also the possible bleeding, calcification, metal deposition might mislead the clinical diagnosis. Paramagnetic Gd^{3+} with seven unpaired electrons and weak longitudinal relaxivity has been proved to be an excellent contrast agent for MRI.[15,45]

The GNa-Er@Nd nanoparticles were evaluated for use as a MR imaging T_1 contrast enhancement agent by a 3T MRI scanner. And the wide-used clinic Gd-DTPA was chosen as a control sample. The contrast capacity of GNa-Er@Nd nanoparticles and Gd-DTPA was studied at different concentrations (0.025- 2.0 mg/mL) with clinical MRI instrument, using deionized water as a control (Figure 9a). In the T_1-weighted MR images, the tubes containing GNa-Er@Nd nanocrystals appeared bright whereas the tubes containing only deionized water remained dark. As the concentration of GNa-Er@Nd nanoparticles increased, the T_1-weighted MR

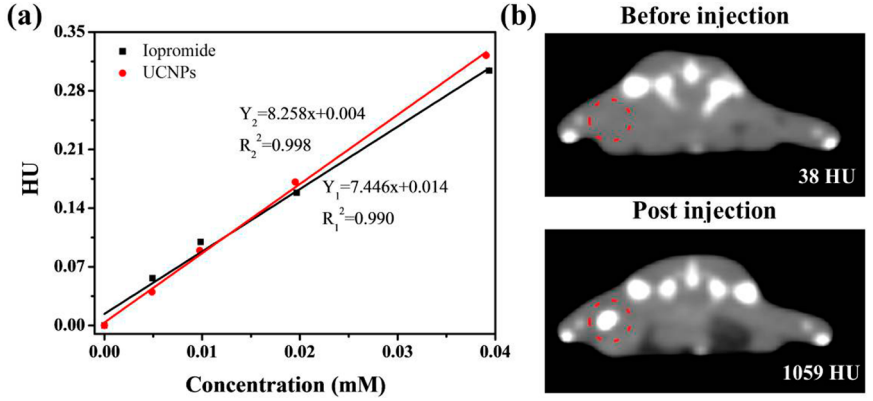

Figure 8. (a) Relaxation rate HU vs various molar concentrations of hydrophilic GNa-Er@Nd and Iopromide at room temperature. (b) CT imaging of a tumor-bearing mouse before and post injection.

DOI: 10.1021/acsami.5b05194
ACS Appl. Mater. Interfaces 2015, 7, 16257−16265

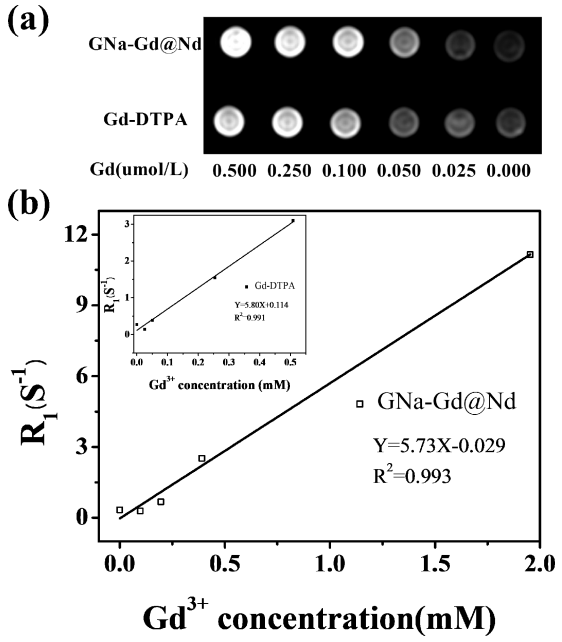

Figure 9. (a) T_1-Weighted and color-mapped MR images of various mass and molar concentrations of GNa-Er@Nd (top) and Gd-DTPA (bottom). Deionized water (0 mg/mL) was the reference. (b) Relaxation rate R_1 $(1/T_1)$ vs various molar concentrations of hydrophilic GNa-Er@Nd and Gd-DTPA (inset) at room temperature using a 3 T MRI scanner.

images gradually turned brighter, i.e. the MR signal intensity increased. The Gd-DTPA exhibited a similar phenomenon as that of GNa-Er@Nd nanoparticles. To study the T_1 contrast effect of GNa-Er@Nd nanoparticles quantitatively, a series of GNa-Er@Nd and Gd-DTPA at different molar concentrations from 0 to 2 mg/mL were investigated for the relaxivity parameters (r_1) under a 3T MRI scanner, confirming the positive signal enhancement ability of GNa-Er@Nd (Figure 9b). There are two good linear relationships between Gd molar concentration in the GNa-Er@Nd and $1/T_1$ (R_1), the slope of each line reflects the relaxation rate of sample, respectively. The r_1 value for Gd-DTPA (in clinical) was 5.80 $s^{-1}\cdot(mM)^{-1}$, which approximated to the values reported in previous literatures.[46] The r_1 value of GNa-Er@Nd was calculated to be 5.73 $s^{-1}\cdot(mM)^{-1}$ and was comparable to that of Gd-DTPA at the same molar concentration.

4. CONCLUSIONS

In conclusion, the multifunctional core−shell GNa-Er@Nd nanoparticles with about 26 nm in diameter were successfully synthesized. The well-defined GNa-Er@Nd nanoparticles showed good monodispersity, water solubility and biocompatibility. Amazingly, the GNa-Er@Nd nanoparticles present brightly dual-wavelength excited upconversion luminescence (UCL) under both 980 and 793 nm laser, excellent relaxivity parameters (r_1) in MRI and Hounsfield units (HU) in CT. These small and monodisperse nanoparticles demonstrated a successful example to integrate multimodal imaging ingredients into one nanoparticle system and opened a door to improve the diagnose quality by multimodal bioimaging.

■ ASSOCIATED CONTENT

Supporting Information

The concentration of rare-earth ions in GNa-Er@Nd nanoparticles measured by ICP-MS, the optical images of all the nanoparticles under different laser excitation, the zeta potentials of GNa-Er@Nd and Er@Nd nanoparticles, and the leakage of Gd^{3+}. The Supporting Information is available free of charge on the ACS Publications website at DOI: 10.1021/acsami.5b05194.

■ AUTHOR INFORMATION

Corresponding Authors

*E-mail: humin1971@mail.xjtu.edu.cn.
*E-mail: hchen@mail.xjtu.edu.cn.

Notes

The authors declare no competing financial interest.

■ ACKNOWLEDGMENTS

This work was supported by the National Natural Science Foundation of China (21174087, 21474079), the Program for New Century Excellent Talents in University (NCET-13-0453), and the Fundamental Funds for the Central Universities (xjj2012001, xjj2014144, xkjc2013002).

■ REFERENCES

(1) Naczynski, D. J.; Sun, C.; Türkcan, S.; Jenkins, C.; Koh, A. L.; Ikeda, D.; Pratx, G.; Xing, L. X-ray-Induced Shortwave Infrared Biomedical Imaging Using Rare-Earth Nanoprobes. *Nano Lett.* **2015**, *15* (1), 96−102.

(2) Shen, J.; Chen, G.; Vu, A.; Fan, W.; Bilsel, O. S.; Chang, C.; Han, G. Engineering the Upconversion Nanoparticle Excitation Wavelength: Cascade Sensitization of Tri-doped Upconversion Colloidal Nanoparticles at 800 nm. *Adv. Opt. Mater.* **2013**, *1*, 644−650.

(3) Niu, X.; Chen, H.; Wang, Y.; Wang, W.; Sun, X.; Chen, L. Upconversion Fluorescence-SERS Dual-Mode Tags for Cellular and in Vivo Imaging. *ACS Appl. Mater. Interfaces* **2014**, *6*, 5152−5160.

(4) Zhang, P.; Cao, J.; Min, Q.; Zhu, J. Multi-Shell Structured Fluorescent−Magnetic Nanoprobe for Target Cell Imaging and On-Chip Sorting. *ACS Appl. Mater. Interfaces* **2013**, *5*, 7417−7424.

(5) Huang, Y.; Wei, T.; Yu, J.; Hou, Y.; Cai, K.; Liang, X. Multifunctional Metal Rattle-Type Nanocarriers for MRI-Guided Photothermal Cancer Therapy. *Mol. Pharmaceutics* **2014**, *11*, 3386−3394.

(6) Liu, Q.; Sun, Y.; Li, C.; Zhou, J.; Li, C.; Yang, T.; Zhang, X.; Yi, T.; Wu, D.; Li, F. ^{18}F-Labeled Magnetic-Upconversion Nanophosphors via Rare-Earth Cation-Assisted Ligand Assembly. *ACS Nano* **2011**, *5*, 3146−3157.

(7) Chen, Q.; Wang, H.; Liu, H.; Wen, S.; Peng, C.; Shen, M.; Zhang, G.; Shi, X. Multifunctional Dendrimer-Entrapped Gold Nanoparticles Modified with RGD Peptide for Targeted CT/MR Dual Modal Imaging of Tumors. *Anal. Chem.* **2015**, *87*, 3949−3956.

(8) Ni, D.; Zhang, J.; Bu, W.; Xing, H.; Han, F.; Xiao, Q.; Yao, Z.; Chen, F.; He, Q.; Liu, J.; Zhang, S.; Fan, W.; Zhou, L.; Peng, W.; Shi, J. Dual-Targeting Upconversion Nanoprobes across the Blood−Brain Barrier for Magnetic Resonance/Fluorescence Imaging of Intracranial Glioblastoma. *ACS Nano* **2014**, *8*, 1231−1242.

(9) Mishra, A.; Mishra, R.; Gottschalk, S.; Pal, R.; Sim, N.; Engelmann, J.; Goldberg, M.; Parker, D. Microscopic Visualization of Metabotropic Glutamate Receptors on the Surface of Living Cells Using Bifunctional Magnetic Resonance Imaging Probes. *ACS Chem. Neurosci.* **2014**, *5*, 128−137.

(10) Klier, D. T.; Kumke, M. U. Upconversion Luminescence Properties of $NaYF_4$:Yb:Er Nanoparticles Codoped with Gd^{3+}. *J. Phys. Chem. C* **2015**, *119*, 3363−3373.

(11) Evans, C. W.; Fitzgerald, M.; Clemons, T. D.; House, M. J.; Padman, B. S.; Shaw, J. A.; Saunders, M.; Harvey, A. R.; Zdyrko, B.;

DOI: 10.1021/acsami.5b05194
ACS Appl. Mater. Interfaces 2015, 7, 16257−16265

Luzinov, I.; Silva, G. A.; Dunlop, S. A.; Iyer, K. S. Multimodal Analysis of PEI-Mediated Endocytosis of Nanoparticles in Neural Cells. *ACS Nano* **2011**, *5*, 8640−8648.
(12) Sandiford, L.; Phinikaridou, A.; Protti, A.; Meszaros, L. K.; Cui, X.; Yan, Y.; Frodsham, G.; Williamson, P. A.; Gaddum, N.; Botnar, R. M.; Blower, P. J.; Green, M. A.; de Rosales, R. T. M. Bisphosphonate-Anchored PEG ylation and Radiolabeling of Superparamagnetic Iron Oxide: Long-Circulating Nanoparticles forin Vivo Multimodal (T1MRI-SPECT) Imaging. *ACS Nano* **2013**, *7*, 500−512.
(13) Groult, H.; Ruiz-Cabello, J.; Pellico, J.; Lechuga-Vieco, A. V.; Bhavesh, R.; Zamai, M.; Almarza, E.; Martín-Padura, I.; Cantelar, E.; Martínez-Alcázar, M. P.; Herranz, F. Parallel Multifunctionalization of Nanoparticles: A One-Step Modular Approach for in Vivo Imaging. *Bioconjugate Chem.* **2015**, *26*, 153−160.
(14) Zhong, Y.; Tian, G.; Gu, Z.; Yang, Y.; Gu, L.; Zhao, Y.; Ma, Y.; Yao, J. Elimination of Photon Quenching by a Transition Layer to Fabricate a Quenching-Shield Sandwich Structure for 800 nm Excited Upconversion Luminescence of Nd^{3+} -Sensitized Nanoparticles. *Adv. Mater.* **2014**, *26* (18), 2831−2837.
(15) Chen, D.; Huang, P. Highly Intense Upconversion Luminescence in Yb/Er:$NaGdF_4$@$NaYF_4$ Core−Shell Nanocrystals with Complete Shell Enclosure of the Core. *Dalton. Trans.* **2014**, *43*, 11299.
(16) Meng, H.; Jin, Z.; Lv, Y.; Yang, C.; Zhang, X.; Tan, W.; Yu, R. Activatable Two-Photon Fluorescence Nanoprobe for Bioimaging of Glutathione in Living Cells and Tissues. *Anal. Chem.* **2014**, *86*, 12321−12326.
(17) Liu, B.; Li, C.; Hou, Z.; Huang, S.; Lin, J. Multifunctional $NaYF_4$:Yb, Er@$mSiO_2$@Fe_3O_4-PEG Nanoparticles for UCL/MR Bioimaging and Magnetically Targeted Drug Delivery. *Nanoscale* **2015**, *7* (5), 1839−48.
(18) Dwivedi, A.; Singh, A. K.; Rai, S. B. Down-Shifting and Upconversion Photoluminescence in Ho^{3+} /Yb^{3+} Codoped $GdNbO_4$: Effect of the Bi^{3+} Ion and the Magnetic Field. *Dalton Trans.* **2014**, *43*, 15906−15914.
(19) Xia, A.; Deng, Y.; Shi, H.; Hu, J.; Zhang, J.; Wu, S.; Chen, Q.; Huang, X.; Shen, J. Polypeptide-Functionalized $NaYF_4$:Yb^{3+}, Er^{3+} Nanoparticles: Red-Emission Biomarkers for High Quality Bioimaging Using a 915 nm Laser. *ACS Appl. Mater. Interfaces* **2014**, *6*, 18329−18336.
(20) Li, Z.; Lv, S.; Wang, Y.; Chen, S.; Liu, Z. Construction of LRET-Based Nanoprobe Using Upconversion Nanoparticles with Confined Emitters and Bared Surface as Luminophore. *J. Am. Chem. Soc.* **2015**, *137*, 3421−7.
(21) Zheng, K.; Qin, W.; Cao, C.; Zhao, D.; Wang, L. NIR to VUV: Seven-Photon Upconversion Emissions from Gd^{3+} Ions in Fluoride Nanocrystals. *J. Phys. Chem. Lett.* **2015**, *6*, 556−560.
(22) Naczynski, D. J.; Sun, C.; Türkcan, S.; Jenkins, C.; Koh, A. L.; Ikeda, D.; Pratx, G.; Xing, L. X-ray-Induced Shortwave Infrared Biomedical Imaging Using Rare-Earth Nanoprobes. *Nano Lett.* **2015**, *15*, 96−102.
(23) Cui, S.; Chen, H.; Zhu, H.; Tian, J.; Chi, X.; Qian, Z.; Achilefu, S.; Gu, Y. Amphiphilic Chitosan Modified Upconversion Nanoparticles for in Vivo Photodynamic Therapy Induced by Near-Infrared Light. *J. Mater. Chem.* **2012**, *22*, 4861−4783.
(24) Lucky, S. S.; Muhammad Idris, N.; Li, Z.; Huang, K.; Soo, K. C.; Zhang, Y. Titania Coated Upconversion Nanoparticles for Near-Infrared Light Triggered Photodynamic Therapy. *ACS Nano* **2015**, *9*, 191−205.
(25) Shen, J.; Chen, G.; Vu, A.; Fan, W.; Bilsel, O. S.; Chang, C.; Han, G. Engineering the Upconversion Nanoparticle Excitation Wavelength: Cascade Sensitization of Tri-doped Upconversion Colloidal Nanoparticles at 800 nm. *Adv. Opt. Mater.* **2013**, *1*, 644−650.
(26) Li, X.; Wang, R.; Zhang, F.; Zhou, L.; Shen, D.; Yao, C.; Zhao, D. Nd^{3+} Sensitized Up/Down Converting Dual-Mode Nanomaterials for Efficient In-vitro and In-vivo Bioimaging Excited at 800 Nm. *Sci. Rep.* **2013**, *3*, 1−7.
(27) Shen, J.; Yang, C.; Dong, L.; Sun, H.; Gao, K.; Yan, X. Incorporation of Computed Tomography and Magnetic Resonance Imaging Function into $NaYF_4$:Yb/Tm Upconversion Nanoparticles for in Vivo Trimodal Bioimaging. *Anal. Chem.* **2013**, *85*, 12166−12172.
(28) Peng, J.; Xu, W.; Teoh, C. L.; Han, S.; Kim, B.; Samanta, A.; Er, J. C.; Wang, L.; Yuan, L.; Liu, X.; Chang, Y. High-Efficiency in Vitro and in Vivo Detection of Zn^{2+} by Dye-Assembled Upconversion Nanoparticles. *J. Am. Chem. Soc.* **2015**, *137*, 2336−2342.
(29) Cheng, C.; Ou, K.; Huang, W.; Chen, J.; Chang, J.; Yang, C. Gadolinium-Based $CuInS_2$ /ZnS Nanoprobe for Dual-Modality Magnetic Resonance/Optical Imaging. *ACS Appl. Mater. Interfaces* **2013**, *5*, 4389−4400.
(30) Zhou, J.; Sun, Y.; Du, X.; Xiong, L.; Hu, H.; Li, F. Dual-Modality in Vivo Imaging Using Rare-Earth Nanocrystals with Near-Infrared to Near-Infrared (NIR-to-NIR) Upconversion Luminescence and Magnetic Resonance Properties. *Biomaterials* **2010**, *31*, 3287−3295.
(31) Deng, Y.; Wang, H.; Gu, W.; Li, S.; Xiao, N.; Shao, C.; Xu, Q.; Ye, L. Ho^{3+} Doped $NaGdF_4$ Nanoparticles as MRI/optical Probes for Brain Glioma Imaging. *J. Mater. Chem. B* **2014**, *2* (11), 1521.
(32) Chen, G.; Ohulchanskyy, T. Y.; Law, W. C.; Ågren, H.; Prasad, P. N. Monodisperse $NaYbF_4$: Tm^{3+}/ $NaGdF_4$ core/shell nanocrystals with near-infrared to near-infrared upconversion photoluminescence and magnetic resonance properties. *Nanoscale* **2011**, *3* (5), 2003.
(33) Zhou, B.; Zheng, L.; Peng, C.; Li, D.; Li, J.; Wen, S.; Shen, M.; Zhang, G.; Shi, X. Synthesis and Characterization of PEGylated Polyethylenimine-Entrapped Gold Nanoparticles for Blood Pool and Tumor CT Imaging. *ACS Appl. Mater. Interfaces* **2014**, *6*, 17190−17199.
(34) Wang, L.; Liu, J.; Dai, Y.; Yang, Q.; Zhang, Y.; Yang, P.; Cheng, Z.; Lian, H.; Li, C.; Hou, Z.; Ma, P. A.; Lin, J. Efficient Gene Delivery and Multimodal Imaging by Lanthanide-Based Upconversion Nanoparticles. *Langmuir* **2014**, *30*, 13042−13051.
(35) Cui, S.; Yin, D.; Chen, Y.; Di, Y.; Chen, H.; Ma, Y.; Achilefu, S.; Gu, Y. In Vivo Targeted Deep-Tissue Photodynamic Therapy Based on Near-Infrared Light Triggered Upconversion Nanoconstruct. *ACS Nano* **2013**, *7*, 676−688.
(36) Zhang, P.; Cao, J.; Min, Q.; Zhu, J. Multi-Shell Structured Fluorescent−Magnetic Nanoprobe for Target Cell Imaging and On-Chip Sorting. *ACS Appl. Mater. Interfaces* **2013**, *5*, 7417−7424.
(37) Peng, J.; Xu, W.; Teoh, C. L.; Han, S.; Kim, B.; Samanta, A.; Er, J. C.; Wang, L.; Yuan, L.; Liu, X.; Chang, Y. High-Efficiency in Vitro and in Vivo. Detection of Zn^{2+} by Dye-Assembled Upconversion Nanoparticles. *J. Am. Chem. Soc.* **2015**, *137*, 2336−2342.
(38) Mariano, R. N.; Alberti, D.; Cutrin, J. C.; Geninatti Crich, S.; Aime, S. Design of PLGA Based Nanoparticles for Imaging Guided Applications. *Mol. Pharmaceutics* **2014**, *11*, 4100−4106.
(39) Abdesselem, M.; Schoeffel, M.; Maurin, I.; Ramodiharilafy, R.; Autret, G.; Clément, O.; Tharaux, P.; Boilot, J.; Gacoin, T.; Bouzigues, C.; Alexandrou, A. Multifunctional Rare-Earth Vanadate Nanoparticles: Luminescent Labels, Oxidant Sensors, and MRI Contrast Agents. *ACS Nano* **2014**, *8*, 11126−11137.
(40) Wang, L.; Xing, H.; Zhang, S.; Ren, Q.; Pan, L.; Zhang, K.; Bu, W.; Zheng, X.; Zhou, L.; Peng, W.; Hua, Y.; Shi, J. A Gd-doped Mg-Al-LDH/Au nanocomposite for CT/MR bimodal imagings and simultaneous drug delivery. *Biomaterials* **2013**, *34* (13), 3390−3401.
(41) Kumar, R.; Nyk, M.; Ohulchanskyy, T. Y.; Flask, C. A.; Prasad, P. N. Combined Optical and MR Bioimaging Using Rare Earth Ion Doped $NaYF_4$ Nanocrystals. *Adv. Funct. Mater.* **2009**, *19* (6), 853−859.
(42) Xie, X.; Gao, N.; Deng, R.; Sun, Q.; Xu, Q.; Liu, X. Mechanistic Investigation of Photon Upconversion in Nd^{3+} -Sensitized Core−Shell Nanoparticles. *J. Am. Chem. Soc.* **2013**, *135*, 12608−12611.
(43) Wang, Y.; Liu, G.; Sun, L.; Xiao, J.; Zhou, J.; Yan, C. Nd^{3+} -Sensitized Upconversion Nanophosphors: Efficient In Vivo Bioimaging Probes with Minimized Heating Effect. *ACS Nano* **2013**, *7*, 7200−7206.
(44) Sun, Y.; Zhu, X.; Peng, J.; Li, F. Core−Shell Lanthanide Upconversion Nanophosphors as Four-Modal Probes for Tumor Angiogenesis Imaging. *ACS Nano* **2013**, *7*, 11290−11300.

DOI: 10.1021/acsami.5b05194
ACS Appl. Mater. Interfaces 2015, 7, 16257−16265

(45) Xing, G.; Yuan, H.; He, R.; Gao, X.; Jing, L.; Zhao, F.; Chai, Z.; Zhao, Y. The Strong MRI Relaxivity of Paramagnetic Nanoparticles. *J. Phys. Chem. B* **2008**, *112* (20), 6288−6291.
(46) Zhang, F.; Braun, G. B.; Pallaoro, A.; Zhang, Y.; Shi, Y.; Cui, D.; Moskovits, M.; Zhao, D.; Stucky, G. D. Mesoporous Multifunctional Upconversion Luminescent and Magnetic "Nanorattle" Materials for Targeted Chemotherapy. *Nano Lett.* **2012**, *12*, 61−67.

DOI: 10.1021/acsami.5b05194
ACS Appl. Mater. Interfaces 2015, 7, 16257−16265